Journal of Materials Chemistry A

Accepted Manuscript

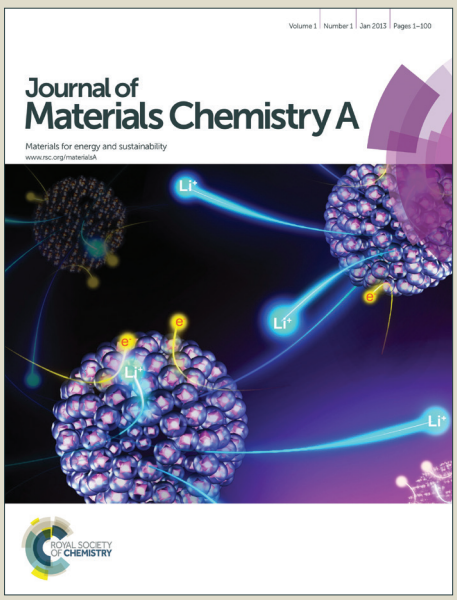

ROYAL SOCIETY OF CHEMISTRY

www.rsc.org/materialsA

Journal of
Materials Chemistry A

RSCPublishing

COMMUNICATION

Platinum-cobalt nanocrystals synthesized under different atmosphere for high catalytic performance of the methanol electro-oxidation

Cite this: DOI: 10.1039/x0xx00000x

Yuchen Qin[a], Xin Zhang[a*], Xiaoping Dai[a], Hui Sun[a], YingYang[a], Qingxiao Shi[a], Daowei Gao[a], Hai Wang[b]

Received ooth January 2012,
Accepted ooth January 2012

DOI: 10.1039/x0xx00000x

www.rsc.org/

Pt–Co nanocrystals with cube, dendrite and sphere have been fabricated in air, hydrogen and nitrogen, respectively, at ambient pressure or 1 MPa. The Pt–Co nanocrystals with chain-like structure synthesized in nitrogen at 1 MPa exhibited superior electrocatalytic activity and stability towards methanol oxidation reaction.

Direct methanol fuel cells (DMFCs) are attracting intense attention due to highly converting chemical energy of methanol directly into electricity without environmental pollution impact.[1,2] Platinum is an excellent electro-catalyst for methanol electro-oxidation but the high cost and easily poisoned by the intermediates are key obstacles for its broad application in fuel cells.[3, 4] Bimetallic alloys of platinum and other transition metals (Co, Fe, Ni, etc.) are expected to substitute platinum owing to the superior catalytic performance and lower cost.[5-14] The catalytic properties of Pt based bimetallic alloys are sensitive dependent on their structures and compositions.[15-24]

The hydrothermal method is the most popular method for synthesizing bimetallic alloys nanocrystals (NCs).[25-28] Much attention has been paid on the influence of organic capping agents and metallic precursors, whereas, the synthesis atmosphere as another significant factor was less reported. In our previous studies,[29,30] we successfully prepared Pt and Pt–Ni NCs bounded by high-index facets (HIFs) using polyvinyl pyrrodine (PVP) and glycine as reducing, dispersing and shape controllers. These results inspired us to investigate whether it is possible to use a similar strategy to synthesize other Pt based binary nanostructures. Herein, we demonstrated one-pot synthesis of Pt–Co alloys with cube, dendrite and sphere in a mixture of H_2PtCl_6, $CoCl_2$, PVP and glycine in air, hydrogen and nitrogen at ambient pressure (AP) (samples were denoted Pt–Co (AAP), Pt–Co (HAP), Pt–Co (NAP)) respectively. To the best of our knowledge, this is the first time to report the synthesis of Pt-Co nanocrystals with cube, dendrite and sphere by tuning the atmosphere and pressure. The Pt–Co NCs were also prepared in air, hydrogen and nitrogen at high pressure (HP) of 1 MPa (samples were denoted Pt–Co (AHP), Pt–Co (HHP), Pt–Co (NHP)). It showed that the synthesis condition of different atmosphere and pressure had significant effect on their structure and composition of Pt–Co NCs. Pt–Co NCs with chain-like structure prepared in nitrogen at 1 MPa exhibited superior electrocatalytic performance towards methanol oxidation reaction.

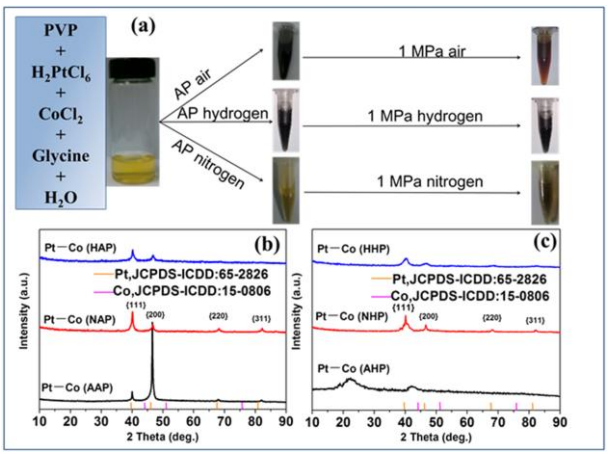

Fig.1 (a) Illustrations of starting and product solutions of Pt–Co NCs. XRD patterns of the products synthesized under air, hydrogen and nitrogen, at (b) AP and (c) HP.

Fig. 1a shows the colour change of the precursor and product solutions of these Pt–Co NCs (before separated via centrifugation). When the synthesis atmosphere was air, the colour of the product solution was black at AP and changed to brownish red as the pressure increased to 1 MPa. This phenomenon revealed that the products synthesized in air at AP and HP were different. When the synthesis atmosphere was hydrogen, the colours of the product solutions prepared at AP and HP were all black. Once using nitrogen instead of hydrogen, we found that the colour of the product solution was yellow

without much discrepancy compared with the precursor solution and the colour was deeper as the pressure increased to 1 MPa. This may imply metallic precursors were reduced more difficultly by the organic reducing agents when synthesized in the nitrogen. The XRD patterns of Pt–Co NCs except Pt–Co (AHP) show the classic reflection of face-centred cubic (fcc) Pt and shift to high angles (Fig. 1b, c).No diffraction signal of Co was detected, indicating the formation of Pt–Co bimetallic alloys. The observation that the Pt–Co (AAP) yield the highest {200} peak intensity, while the Pt–Co (NAP), Pt–Co (HAP), Pt–Co (NHP) and Pt–Co (HHP) exhibit the enhanced {111} peak intensity. The enhanced {200} peak intensity further confirms that the Pt–Co (AAP) have a {100}-dominated cubic morphology with very narrow shape distributions.[31] It is found that Pt–Co (NHP) NCs feature a broadened {111} peak compared with Pt–Co (NAP), indicating that the size of Pt–Co (NHP) NCs is smaller than that of Pt–Co (NAP) NCs according to Debye-Scherer formula. The similar change of {111} peak can also be observed on the XRD patterns of Pt–Co (HHP) and Pt–Co (HAP). Whereas, the XRD pattern of Pt–Co (AHP) shows two diffraction peaks at 2 theta of 22.3^{o} and 42.1^{o}, featuring reflections of PtO_2 and CoO (JCPDS-ICDD cards: 38-1355, 43-1004), respectively. Clearly, the metallic Pt–Co alloy had not been obtained in the 1 MPa of air.

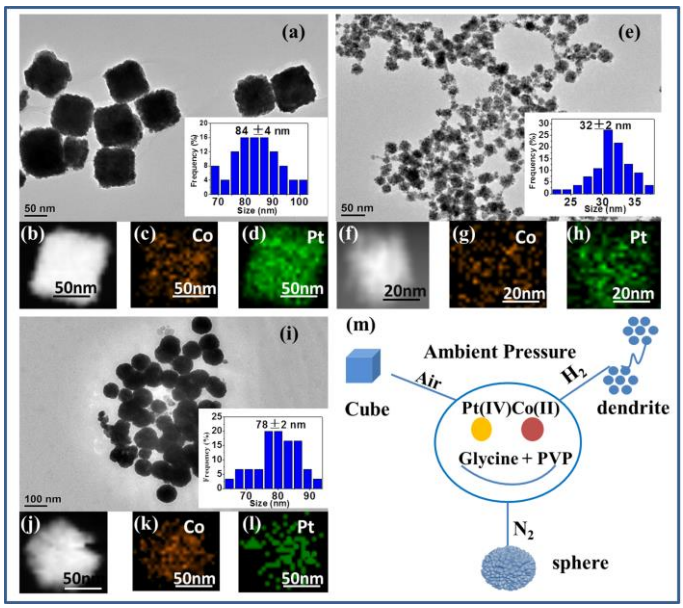

Fig.2 Representative TEM images (and size-distribution histograms) of Pt-Co NCs were prepared at atmospheric pressure of (a) air, (e) hydrogen, (i) nitrogen. (b), (f) and (j) HAADF-STEM images. (c), (d), (g), (h), (k) and (l) EDS-mapping images. (m) The schematic model sketch for the products synthesized under atmosphere at AP.

Fig. 2 shows the representative transmission electron microscopy (TEM) images of Pt–Co alloy NCs under air, hydrogen and nitrogen at AP. The high selectivity (>90%) of nanocubic Pt–Co alloy NCs were observed in air at AP (Fig. 2a).The cubic NCs were attached with much small particles. The average edge length of the Pt–Co nanocubes was 84±4 nm. The products synthesized in hydrogen at AP were dendritic shape with high selectivity (>95%) (Fig. 2e). It seemed that the dendritic Pt–Co (HAP) NCs were formed with small spherical particles. The average size of Pt–Co (HAP) dendritic NCs was determined as the largest distance between two points on a single dendritic particle and was found to be 32 ± 2 nm. Specifically, the diameter of the small spherical-like particle is 4 nm. Once using nitrogen instead of hydrogen, the morphology of as-prepared products changed from dendrites to spheres. The average diameter of each spherical Pt–Co (NAP) NCs is 78 ± 2 nm (Fig. 2i). The high-resolution TEM (HRTEM) images reveal the lattice spacing of Pt–Co (HAP) and Pt–Co (NAP) is 0.223 nm and 0.222 nm respectively, which is smaller than 0.227 nm corresponding to the {111} facet of fcc Pt, confirming that the formation of Pt–Co NCs (See Fig. S1). These morphologies of Pt–Co NCs were demonstrated by high-angle annular dark-field scanning TEM (HAADF-STEM) (Fig. 2b, f and j). Nanoscale elemental mapping revealed that Pt and Co were distributed uniformly throughout the cubes, dendrites and spheres (Fig. 2c, d and g, h and k, l). The synthetic strategy was illustrated in Fig. 2m.

Hydrothermal synthesis under air is a typical synthetic condition. Glycine was reported to play the vital role of tuning the nucleation and growth rates of Pt–Co NCs and PVP was a polymeric capping agent whose oxygen atoms bind most strongly to the {100} facets resulting in shape-controlled function corporately.[32,33] As well known, Hydrogen is a strong reducing atmosphere. When using hydrogen instead of air and maintaining other reaction conditions unchanged, it was reasonable that the reduction rate of Pt(IV) and Co(II) precursors and the nucleation rates of Pt–Co NCs became faster. A large number of small particles with average size of 4 nm formed under the dispersion of PVP. Finally, the dendritic Pt–Co NCs could be formed through the reaction-limited aggregation (RLA) of spherical nanoparticles.[34] When nitrogen was brought in the synthesis system, the process of reduction was more difficult and the nucleation rate was slower because of the inert environment. Due to no oxygen was added, multiply twinned seeds would be formed and evolved into spherical particles through anisotropic growth finally.[35]

Fig. 3a shows TEM images of Pt–Co NCs obtained under air at 1MPa. Clearly, the spindle flake-like morphology of Pt–Co (AHP) NCs is dramatically different from the nanocubic shape of Pt–Co (AAP) NCs. The average length of Pt–Co (AHP) NCs is 98±2 nm and the average width is 62±4 nm. The result of XRD indicated that the oxidation state of Pt(IV) precursor and Co(II) precursor were remained under 1 MPa of air. Pt–Co dendritic NCs can be remained in hydrogen at 1 MPa (Fig. 3b).The average diameter of spherical particles is also 4 nm but the average size of the dendritic NCs is 18±2 nm, which was smaller than that (32 ± 2 nm) of Pt–Co (HAP) NCs. Compared with the structure of Pt–Co (HAP), there was a tendency that the structure transformed from compact clusters to open structure as pressure increased. Remarkably, the structure changed from their regular layout of spherical aggregation of Pt–Co (NAP) to regular chain-like arrangement of Pt–Co (NHP) as the increased pressure of nitrogen. Pt–Co (NHP) NCs was also changed to quasi-sphere (Fig. 3c). The average size of these NCs is 34±2 nm, which is much smaller than the size of Pt–Co (NAP) NCs. The

formation of chain-like structure could be due to the dipole-dipole interactions between the Pt–Co (NHP) NCs.[36] Compressed nitrogen was used as the drive force for formation of the chain-like structure. It could break the balance between attractive van der Waals potentials and the residual electrostatic repulsions, leading to increase the chance of Brownian collisions. Then dipole-dipole attraction should play the role of forming linear chains of single Pt–Co NCs to minimize enthalpy of the system by promoting dipole alignment and decrease inter dipole distances, resulting in formation of the chain-like structure finally.[37] HAADF-STEM shows that there are some porous structures existing in each Pt–Co (NHP) NCs (see Fig. 3d and Fig. S2). To better resolve the shapes and structure of Pt–Co (NHP) NCs, we took HRTEM images. The observed lattice spacing of 0.222 nm is smaller than 0.227 nm corresponding to the {111} facet of fcc Pt, indicating a contraction of the lattice upon substitution of Pt with Co and formation of Pt–Co bimetallic alloys (see Fig. 3e).[38] In addition, these {111} lattice fringes are not continuous, their orientations are different, and the crystal boundaries between the quasi-spherical NCs can be clearly observed. A lot of crystalline defects including the interfacial dislocation, intragranular dislocation, and crystal face defects have been found on the chain-like structural Pt–Co (NHP) NCs (see Fig. 3f–3i). The Pt atoms on these defects are regarded as highly active sites for catalysis, which could make great contributions to excellent electrocatalytic activity.[11,39]

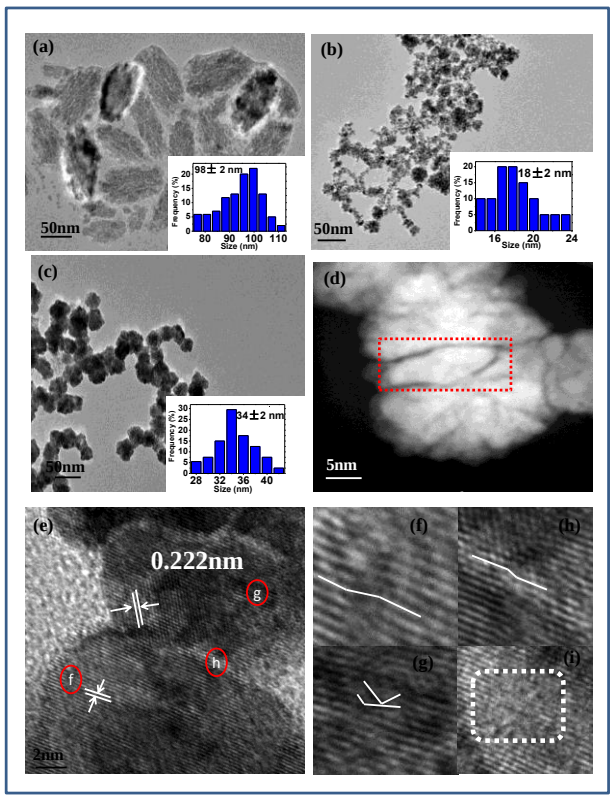

Fig.3 Representative TEM images of Pt–Co NCs synthesized at 1 MPa of (a) air, (b) hydrogen, (c) nitrogen and (d) HAADF-STEM images and (e) HRTEM images of products synthesized in nitrogen at 1 MPa, and (f), (g)intragranular dislocation,(h)interfacial dislocation and (i) crystal face defects.

Table 1 The chemical composition of Pt–Co NCs measured by ICP-AES

Sample	Pt–Co (AAP)	Pt–Co (HAP)	Pt–Co (HHP)	Pt–Co (NAP)	Pt–Co (NHP)
Pt_xC_{Oy}	$Pt_{86}Co_{14}$	$Pt_{44}Co_{56}$	$Pt_{51}Co_{49}$	$Pt_{13}Co_{87}$	$Pt_{15}Co_{85}$

It is found that various atmospheres can be used to control the composition of Pt–Co alloy NCs without changing the initial precursor amount. The composition of Pt–Co alloy NCs determined by inductively coupled plasma atomic emission spectroscopy (ICP-AES) changed from $Pt_{86}Co_{14}$ of Pt–Co (AAP) to $Pt_{13}Co_{87}$ of Pt–Co (NAP) and $Pt_{44}Co_{56}$ of Pt–Co (HAP) (shown in Table1). Clearly, the order of Pt weight of Pt–Co NCs follows air atmosphere > hydrogen atmosphere > nitrogen atmosphere. While, the Pt and Co compositions changed very little as the pressure increased under a certain atmosphere. The differences of composition are likely associated with atmosphere-dependent chemical reduction rates of Pt(IV) and Co(II).[22] Ultraviolet–visible spectroscopy (UV-Vis) reveals Pt(IV) has the strongest coordination interaction with glycine under nitrogen when Pt(IV) was added to glycine aqueous solution (see Fig. S3a). However, Co(II) has weak coordination interaction with glycine under nitrogen (see Fig. S3b). In addition, the colour of product solution is yellow indicating a lot of Pt precursors were not reduced and remained in the solution. Therefore, we deduce that the reduction rate of Pt(IV) is slowest under nitrogen atmosphere, which leading to the lowest Pt content in Pt–Co alloy NCs.

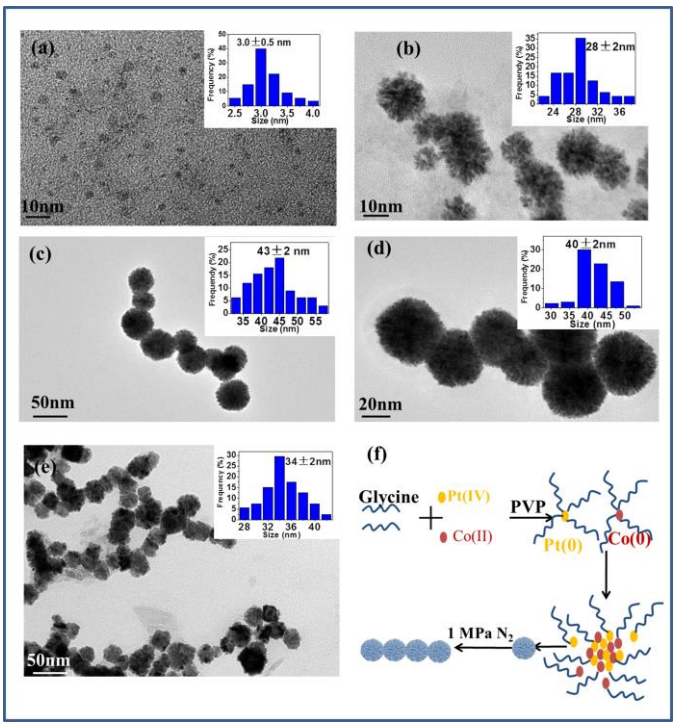

Fig.4 TEM and size distribution (insert) images demonstrating the course of morphological evolution for Pt–Co alloy NCs synthesized in nitrogen at 1 MPa. The reaction time is (a) 20min, (b) 2h, (c) 3h (d) 4h and (e) 7h, (f) the schematic model diagram for the assembly process of Pt–Co (NHP).

Considering the slower nucleation and growth rate of Pt–Co alloy NCs synthesized under nitrogen, it is helpful for investigation of the evolution process. The course of morphological evolution of Pt–Co alloy NCs synthesized in nitrogen at 1 MPa was illustrated in Fig. 4. Large number of tiny spherical NCs with an average size of 3.0 nm occurred at 20 min (Fig. 4a). As the time increased to 2 h, most of these tiny spherical NCs aggregated together forming the flower-like NCs and the average size were 28 nm. Notably, small spherical NCs were clearly observed in the flower-like structure (Fig. 4b). As the evolution process continued, the tiny NCs aggregated more closely. An average size of 43 nm and 40 nm Pt–Co flower-like NCs had been produced at 3h and 4h (Fig. 4c, d). The small spherical NCs could still be discerned. Finally, Well-defined quasi-spherical Pt–Co NCs had been prepared at 7h. The small spherical NCs could hardly be observed in these quasi-spheres. Interestingly, the average size of the quasi-spherical Pt–Co NCs had decreased to 34 nm (Fig. 4e). The time sequential evolution experiment clearly demonstrated that the Pt–Co alloy quasi-spheres were formed by a self-assembly process (Fig. 4f). The role of glycine played as soft-templates to confine the growth of Pt–Co alloy NCs due to the strongest interactions between amine and Pt(IV) or Co(II) species under nitrogen (Fig. S3) and PVP was known to be a hydrogen bond acceptor which induced self-assembly to form quasi-spherical Pt–Co NCs synthesized in nitrogen at 1 MPa.[30,40,41] The decrease in the average size from 40 nm to 34 nm can be ascribed to the formation of well-defined Pt–Co alloy quasi-spheres during the self-assembly process, which the tiny spherical NCs aggregated too closely to be discerned.

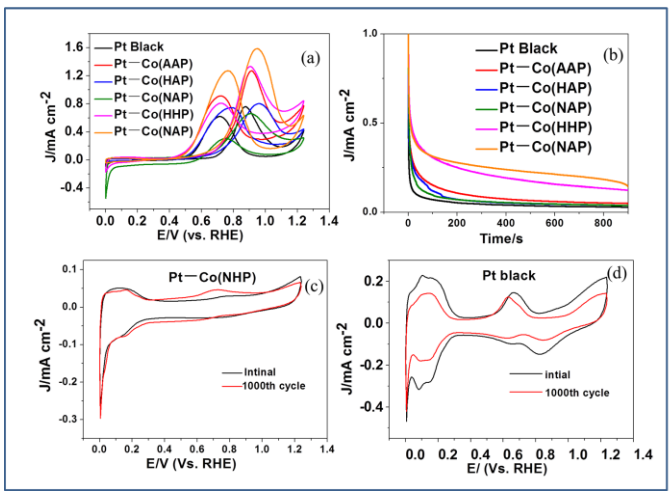

Fig.5 (a) Cyclic voltammograms and (b) i-t curves (at 0.6V Vs. RHE) of Pt–Co alloy NCs and commercial Pt black in 0.5 M H_2SO_4+2.0 M CH_3OH solution at a scan rate of 50mV/s. Cyclic voltammograms of (c) Pt–Co(NHP) NCs and (d) commercial Pt black in 0.5 M H_2SO_4 solution at a scan rate of 50mV/s.

The as-synthesized Pt–Co alloy NCs have been measured in the electro-oxidation of methanol to probe the structure effects on electro-catalytic properties. For comparison, commercial Pt black as the reference, was tested under the same conductions. Before each electrochemical test, the electrode after dipping the Pt–Co alloy NCs was illuminated by UV lamp for 12 h to further remove the capping agents by UV-ozone (UVO) cleaning as described in our earlier work.[41] Fig. 5a shows the cyclic voltammograms (CVs) for electro-oxidation of methanol on Pt–Co alloy NCs and commercial Pt black catalysts. The specific current density (Js) was normalized to the electro-chemically active surface area (ECSA), which was tested by integrating the electric charges on the adsorption/desorption peak of hydrogen regions in CVs measured in fresh nitrogen-saturated 0.5 M H_2SO_4 solution (see Fig. S4). The peak current density of methanol oxidation in the positive potential scan was 1.27, 0.80, 0.66, 1.34, 1.60, and 0.76 mA cm^{-2}, respectively, on the Pt–Co (AAP), Pt–Co (HAP), Pt–Co (NAP), Pt–Co(HHP), Pt–Co (NHP) and commercial Pt black. The oxidation current density on Pt–Co(AAP), Pt–Co(HAP), Pt–Co(NAP), Pt–Co(HHP), and Pt–Co(NHP) are almost 1.7, 1.1, 0.87 1.8 and 2.0 times than that of commercial Pt black. It is evident that the Pt–Co NCs prepared in nitrogen at 1 MPa exhibited the highest specific activity among these catalysts. In addition, the specific activity of Pt–Co(NHP) (1.60 mA cm^{-2}) is higher than those of previous reported Pt–Co alloyed catalysts (1.50 mA cm^{-2}, 0.1 M $HClO_4$+1.0 M CH_3OH) [38] and Pt concave nanocubes[29] (1.19 mA cm^{-2}, 0.5 M H_2SO_4+2.0 M CH_3OH). It is also found that the electro-catalytic activity of Pt–Co NCs prepared under HP is higher than that of Pt–Co NCs synthesized at AP. The difference in the specific activity of Pt–Co alloy NCs could be due to their differences of nanostructures and compositions. Because the structure of Pt–Co (HHP) is more open than that of Pt–Co (HAP) and the size of Pt–Co (HHP) dendrites is much smaller than Pt–Co (HAP) dendrites. Therefore more exposed atoms exist on the structure of Pt–Co (HHP) NCs. It makes the great contributions to the superior specific activity. For the structure of Pt–Co (NHP), the existence of porous structures in the quasi-spherical NCs increased the accessibility and utilization of Pt atoms. In addition, there are a lot of crystal defect sites on Pt–Co (NHP) NCs and Pt atoms on crystal defect site are regarded as highly active sites for catalysis.[11,43] These unique properties of Pt–Co (NHP) resulted in excellent specific activity. The lowest Pt content ($Pt_{15}Co_{85}$) further demonstrated the advantageous of the unique structure for methanol electrooxidation. Notably, it was found that Pt–Co (HHP) NCs performed superior mass activity compared with Pt black (see Fig S5). Compared with mass activity of previous reported Pt_3Co nanoflowers (0.385A mg^{-1}, 0.1 M $HClO_4$+1.0 M CH_3OH),[44] the mass activity of Pt–Co (HHP) NCs (0.509A mg^{-1}) exhibited superior methanol electrooxidation activity. It could be due to Pt–Co (HHP) dendritic NCs with open structure, which were composed of tiny spherical Pt–Co NCs of 4nm. To further evaluate the stability of these Pt–Co alloy NCs, i-t curves were conducted for 900 s (Fig. 5b). It's seen that these Pt–Co alloy NCs possess superior stability during the electrochemical measurements, as compared with commercial Pt black catalysts. Furthermore, the CVs of Pt–Co (NHP) and commercial Pt black catalysts were carried out in 0.5 mol/L H_2SO_4 solution (Fig. 5c, d). It is observed that the ECSA of Pt–Co (NHP) reserved almost 90% of its initial ECSA after a durability test of 1000 cycles while the ECSA of commercial Pt black dropped to almost 50% under the same conditions. This is an additional evidence to support the better stability of Pt–Co alloy NCs than commercial Pt black catalyst.

Conclusions

In summary, Pt–Co alloy NCs have been prepared under various atmospheres (air, nitrogen and hydrogen) with different pressure. The structure of Pt–Co NCs is sensitive to the atmosphere and pressure. Pt–Co nanocubes were synthesized in air at atmosphere pressure, while flake-like PtO_2 and CoO NCs were produced in air at 1 MPa. Pt–Co dendritic NCs were both prepared in hydrogen at atmosphere pressure and 1 MPa of air. But the structure of Pt–Co (HHP) is more open than that of Pt–Co (HAP). Pt–Co spherical NCs with an average size of 78 nm were aggregated irregularly when synthesized in nitrogen at AP but presented regular chain-like structure as the pressure of nitrogen increased to 1 MPa. Pt–Co alloy NCs prepared under hydrogen of 1 MPa and nitrogen showed superior specific activity and stability in comparison with commercial Pt black in the electro-oxidation of methanol due to their unique nanostructures.

Acknowledgments

The authors acknowledge the financial supports from the NSFC (Nos.20903119, 21173269, 91127040) and Ministry of Science and Technology of China (No. 2011BAK15B05) and Specialized Research Fund for the Doctoral Program of Higher Education (20130007110003).

[a]State Key Laboratory of Heavy Oil Processing, China University of Petroleum,Beijing102249,P.R. China.

[b]National Institute of Metrology, Beijing 100013, China.

E-mail: zhangxin@cup.edu.cn

† Electronic supplementary information (ESI) available: experimental section and results of HAADF-STEM,UV-vis and ICP-AES analyses, and electrocatalysis data.

References

1. M. S. Dresselhaus and I. L. Thomas, *Nature*, 2001, **414**, 332-337.
2. B. C. H. Steele and A. Heinzel, *Nature*, 2001, **414**, 345-352.
3. M. C. Orilall, F. Matsumoto, Q. Zhou, H. Sai, H. D. Abruña, F. J. DiSalvo and U. Wiesner, *J. Am. Chem. Soc.*, 2009, **131**, 9389-9395.
4. C. Chen, Y. Kang, Z. Huo, Z. Zhu, W. Huang, H. L. Xin, J. D. Snyder, D. Li, J. A. Herron, M. Mavrikakis, M. Chi, K. L. More, Y. Li, N. M. Markovic, G. A. Somorjai, P. Yang and V. R. Stamenkovic, *Science*, 2014, **343**, 1339-1343.
5. C. Zhang, S. Y. Hwang and Z. Peng, *J. Mater. Chem. A*, 2014, **2**, 19778-19787.
6. H. Li, H. Lin, Y. Hu, H. Li, P. Li and X. Zhou, *J. Mater. Chem.*, 2011, 21, 18447-18453.
7. J. Wu, L. Qi, H. You, A. Gross, J. Li and H. Yang, *J. Am. Chem. Soc.*, 2012, **134**, 11880-11883.
8. M. K. Carpenter, T. E. Moylan, R. S. Kukreja, M. H. Atwan and M. M. Tessema, *J. Am. Chem. Soc.*, 2012, **134**, 8535-8542.
9. P. Ferrin and M. Mavrikakis, *J. Am. Chem. Soc.*, 2009, **131**, 14381-14389.
10. C. Gumeci, D. U. Cearnaigh, D. J. Casadonte and C. Korzeniewski, *J. Mater. Chem. A*, 2013, **1**, 2322-2330.
11. Z. Guo, X. Dai, Y. Yang, Z. Zhang, X. Zhang, S. Mi, K. Xu and Y. Li, *J. Mater. Chem. A*, 2013, **1**, 13252-13260.
12. Q. Sun, Z. Ren, R. Wang, N. Wang and X. Cao, *J. Mater. Chem.*, 2011, **21**, 1925-1930.
13. G.-T. Fu, R.-G. Ma, X.-Q. Gao, Y. Chen, Y.-W. Tang, T.-H. Lu and J.-M. Lee, *Nanoscale*, 2014, **6**, 12310-12314.
14. G.-T. Fu,, L. Ding, Y. Chen, J. Lin, Y. Tang and T. Lu, *CrystEngComm*, 2014, **16**, 1606-1610.
15. N. S. Porter, H. Wu, Z. Quan and J. Fang, *Acc. Chem. Res.*, 2013, **46**, 1867-1877.
16. Y. Kang, J. B. Pyo, X. Ye, T. R. Gordon and C. B. Murray, *ACS Nano*, 2012, **6**, 5642-5647.
17. K. Y. Lee, Y. W. Lee, M. Kim and T. H. Kim, *J. Mater. Chem. A*, 2014, **2**, 2735-2741.
18. X.-Y. Liu, Y. Zhang, M.-X. Gong, Y.-W. Tang, T.-H. Lu, Y. Chen and J.-M. Lee, *J. Mater. Chem. A*, 2014, **2**, 13840-13844.
19. H. Meng, F. Xie, J. Chen, S. Sun and P. K. Shen, *Nanoscale*, 2011, **3**, 5041-5048.
20. L.-L. Wang, D.-F. Zhang and L. Guo, *Nanoscale*, 2014, **6**, 4635-4641.
21. X. Huang, Y. Chen, E. Zhu, Y. Xu, X. Duan and Y. Huang, *J. Mater. Chem. A*, 2013, **1**, 14449-14454.
22. Y. Wang, Y. Zhu, J. Chen and Y. Zeng, *Nanoscale*, 2012, **4**, 6025-6031.
23. M. Gong, G. Fu, Y. Chen, Y. Tang and T. Lu, *ACS Applied Materials & Interfaces*, 2014, **6**, 7301-7308.
24. J. Xu, X. Liu, Y. Chen, Y. Zhou, T. Lu and Y. Tang, *J. Mater. Chem.*, 2012, **22**, 23659-23667.
25. C. Wang, N. M. Markovic and V. R. Stamenkovic, *ACS Catalysis*, 2012, **2**, 891-898.
26. C. Cui, L. Gan, M. Neumann, M. Heggen, B. Roldan Cuenya and P. Strasser, *J. Am. Chem. Soc.*, 2014, **136**, 4813-4816.
27. F. Somodi, S. Werner, Z. Peng, A. B. Getsoian, A. N. Mlinar, B. S. Yeo and A. T. Bell, *Langmuir*, 2012, **28**, 3345-3349.
28. J. Gu, Y.-W. Zhang and F. Tao, *Chem. Soc. Rev.*, 2012, **41**, 8050-8065.
29. Z. Zhang, J. Hui, Z.C. Liu, X. Zhang, J. Zhuang and X. Wang, *Langmuir*, 2012, **28**, 14845-14848.
30. X. Xu, X. Zhang, H. Sun, Y. Yang, X. Dai, J. Gao, X. Li, P. Zhang, H.-H. Wang, N.-F. Yu and S.-G. Sun, *Angew. Chem. Int. Ed.*, 2014, **53**, 12522-12527.
31. J. Zhang and J. Fang, *J. Am. Chem. Soc.*, 2009, **131**, 18543-18547.
32. Z. Zhang, Y. Yang, F. Nosheen, P. Wang, J. Zhang, J. Zhuang and X. Wang, *Small*, 2013, **9**, 3063-3069.
33. Y. Sun, B. Mayers, T. Herricks and Y. Xia, *Nano Lett.*, 2003, **3**, 955-960.
34. Q. Yuan, D.-B. Huang, H.-H. Wang and Z.-Y. Zhou, *Langmuir*, 2014, **30**, 5711-5715.
35. Y. Xiong, J. Chen, B. Wiley, Y. Xia, S. Aloni and Y. Yin, *J. Am. Chem. Soc.*, 2005, **127**, 7332-7333.
36. Z. Tang, N. A. Kotov and M. Giersig, *Science*, 2002, **297**, 237-240.
37. C. C. Li, W. Zhang, H. Ang, H. Yu, B. Y. Xia, X. Wang, Y. H. Yang, Y. Zhao, H. H. Hng and Q. Yan, *J. Mater. Chem. A*, 2014, **2**, 10676-10681.
38. H. Yang, J. Zhang, K. Sun, S. Zou and J. Fang, *Angew. Chem.*, 2010, **122**, 7000-7003.
39. A.-X. Yin, X.-Q. Min, Y.-W. Zhang and C.-H. Yan, *J. Am. Chem. Soc.*, 2011, **133**, 3816-3819.
40. H. You, S. Yang, B. Ding and H. Yang, *Chem. Soc. Rev.*, 2013, **42**, 2880-2904.
41. L. Wang, S. Cui, Z. Wang, X. Zhang, M. Jiang, L. Chi and H. Fuchs, *Langmuir*, 2000, **16**, 10490-10494.
42. Z.C. Zhang, J.F. Hui, Z.G. Guo, Q.-Y. Yu, B. Xu, X. Zhang, Z.-C. Liu, C.M. Xu, J.S. Gao and X. Wang, *Nanoscale*, 2012, **4**, 2633-2639.
43. Z. C. Zhang, X. Zhang, Q. Y. Yu, Z. C. Liu, C. M. Xu, J. S. Gao, J. Zhuang and X. Wang,Chem.Eur. J., 2012, 18, 2639.
44. J.-N. Zheng, L.-L. He, C. Chen, A.-J. Wang, K.-F. Ma and J.-J. Feng, *J. Power Sources*, 2014, **268**, 744-751.

Graphic Abstract

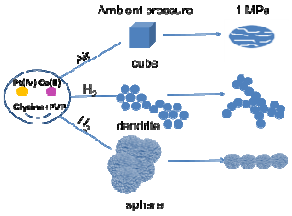

Pt–Co nanocrystals were shape-controlled synthesized with cubes, dendrites and spheres by varying the atmosphere and pressure.